JACS
JOURNAL OF THE AMERICAN CHEMICAL SOCIETY
Article
pubs.acs.org/JACS

Durable Carbon-Coated Li_2S Core–Shell Spheres for High Performance Lithium/Sulfur Cells

Caiyun Nan,[†,‡,§] Zhan Lin,[†,‡] Honggang Liao,[∥] Min-Kyu Song,[⊥] Yadong Li,[§] and Elton J. Cairns*[,†,‡]

[†]Department of Chemical and Biomolecular Engineering, University of California, Berkeley, California 94720, United States
[‡]Environmental Energy Technologies Division, Lawrence Berkeley National Laboratory, Berkeley, California 94720, United States
[§]Department of Chemistry, Tsinghua University, Beijing, 100084, P. R. China
[∥]Materials Sciences Division, Lawrence Berkeley National Laboratory, Berkeley, California 94720, United States
[⊥]The Molecular Foundry, Lawrence Berkeley National Laboratory, Berkeley, California 94720, United States

Supporting Information

ABSTRACT: Lithium sulfide (Li_2S) is an attractive cathode material with a high theoretical specific capacity (1166 mAh g^{-1}). However, the poor cycle life and rate capability have remained significant challenges, preventing its practical application. Here, Li_2S spheres with size control have been synthesized for the first time, and a CVD method for converting them into stable carbon-coated Li_2S core–shell (Li_2S@C) particles has been successfully employed. These Li_2S@C particles with protective and conductive carbon shells show promising specific capacities and cycling performance with a high initial discharge capacity of 972 mAh g^{-1} Li_2S (1394 mAh g^{-1} S) at the 0.2C rate. Even with no added carbon, a very high Li_2S content (88 wt % Li_2S) electrode composed of 98 wt % 1 μm Li_2S@C spheres and 2 wt % binder shows rather stable cycling performance, and little morphology change after 400 cycles at the 0.5C rate.

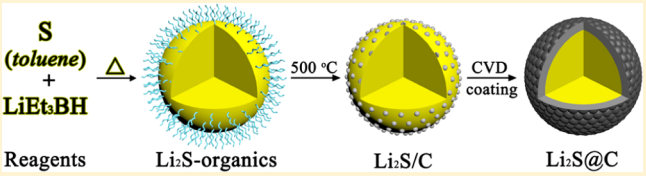

INTRODUCTION

As current cathode materials for lithium ion cells approach an intrinsic specific capacity limit of less than 300 mAh g^{-1}, new generations of rechargeable cathodes with high specific capacity are urgently needed.[1−3] Sulfur is a promising candidate which has a high theoretical specific capacity of 1675 mAh g^{-1} as well as very low cost, high abundance, and low environmental impact.[3−6] Significant progress has been made to improve the utilization of sulfur and alleviate the capacity fading by size control of the sulfur particles,[7−11] coatings on sulfur particles,[11−14] use of sulfur–carbon composites,[15−24] trapping of polysulfides,[25−28] and electrolyte modification.[29−32] However, for use with the sulfur cathode, lithium metal or a lightweight lithiated anode is essential for high specific energy. Lithium metal typically forms dendrites in conventional organic solvent-based electrolytes, causing shorting and safety concerns. Furthermore, some of the protective coatings on sulfur particles may be easily destroyed because sulfur undergoes a volume expansion of ~76% when totally converted to Li_2S.

Considering the challenges for the sulfur cathode, fully lithiated sulfur, lithium sulfide (Li_2S), is an attractive cathode material for lithium/sulfur (Li/S) cells, with a theoretical specific capacity of 1166 mAh g^{-1}. It can be paired with different kinds of lithium metal free materials, such as the high capacity silicon anode. Moreover, compared with sulfur, Li_2S has a higher melting point and is in the maximum volume state, so modifications on Li_2S materials can be performed at a higher temperature and the surface coating can be more stable. Nevertheless, the problems of low electronic conductivity, and the solubility of polysulfides in many electrolytes still exist for the Li_2S cathode. Thus, it is also essential to use carbon-containing composites, control particle size, and provide protection for the Li_2S active material. A protective and conductive shell on the surface of small Li_2S particles, which will not be broken by expansion during discharge, seems to be a candidate solution for using Li_2S material in Li/S cells. Recently, some exciting results concerning Li_2S cathodes were reported.[33−42] However, most of the reports are based on commercial Li_2S powder or commercial Li_2S subjected to ball-milling, resulting in random particle sizes and morphologies, not ideal for surface coatings. There are almost no reports of synthesized Li_2S with uniform particle size and morphology so far.

Herein, we report for the first time an easy strategy to synthesize Li_2S spheres with size control. We have prepared three different sizes, 2 μm, 1 μm, and 500 nm, which can be the core material for a variety of coating methods. In this paper, these three sizes of Li_2S spheres are successfully coated with carbon by the CVD method to form stable carbon-coated Li_2S core–shell (Li_2S@C) structures that show promising specific capacities and cycling performance with a high initial discharge capacity of 972 mAh g^{-1} Li_2S (1394 mAh g^{-1} S) at the 0.2C rate (1C = 1166 mA g^{-1} Li_2S) and good capacity retention after

Received: December 19, 2013
Published: February 28, 2014

dx.doi.org/10.1021/ja412943h | J. Am. Chem. Soc. 2014, 136, 4659−4663

100 cycles. When no carbon black was added to the electrode mixture, a very high Li_2S content (88 wt % Li_2S) electrode composed of 98 wt % 1 μm Li_2S@C spheres and 2 wt % binder showed rather stable cycling performance, and little morphology change after 400 cycles.

RESULTS AND DISCUSSION

The chemical reaction for the synthesis of Li_2S is indicated in eq 1.[43]

$$S + 2LiEt_3BH = Li_2S + 2Et_3B + H_2 \quad (1)$$

Sulfur was first dissolved in toluene and then added into a solution of lithium triethylborohydride ($LiEt_3BH$) in tetrahydrofuran (THF). After the THF was removed by heat treatment, stable Li_2S spheres were formed. More information about the synthesis of Li_2S spheres is presented in the Supporting Information.

XRD and Raman spectra of the as-prepared Li_2S spheres are shown in Figure 1a and 1b. The X-ray diffraction (XRD) spectrum shows that a pure Li_2S powder was formed (JCPDS card no. 23-0369) by the reaction of sulfur with $LiEt_3BH$. However, in the Raman spectrum, besides showing the characteristic peak of Li_2S at ~370 cm^{-1}, several C−H, C−S, S−H, and S−O bonds were detected between 700 and 1500 cm^{-1},[44,45] which reflect the existence of an organic residue in the powder. To remove the organics, the as-synthesized white Li_2S spheres were heat treated in an argon atmosphere at 500 °C for 0.5 h (labeled as Li_2S-500 °C). After the 500 °C heat treatment, the white Li_2S spheres became a fine gray powder, and the sharp XRD peaks reveal an enhanced crystallization of the Li_2S particles as shown in Figure 1a. The Raman spectra in Figure 1b show that after heat treatment all the peaks of the organic residue were gone. Instead, new Raman peaks corresponding to the D band and G band of carbon were found. In addition, the intensity of the Li_2S peak was reduced. These spectra indicate that the organic residue was converted to carbon and covered some parts of the Li_2S particles. In order to increase the conductivity of the Li_2S powder as well as protect the Li_2S particles from sulfur (polysulfide) loss during the electrochemical reaction, the Li_2S-500 °C material was further coated with carbon by the CVD method using acetylene gas to form a carbon-coated Li_2S core−shell structure (labeled as Li_2S@C). As observed in our experiments (Supporting Information Figure S1), although the CVD is conducted under argon protection, there is still a risk of side reactions of Li_2S at higher temperatures (impurities in argon gas or trace moisture). Thus, a relatively low temperature was chosen for deposition of the carbon coating on the Li_2S. Considering that the decomposition rate of C_2H_2 at 400 °C is very slow, 450 °C was chosen for acetylene decomposition. The thickness of the coatings is controlled by the time of exposure to the Ar−acetylene gas mixture at the deposition temperature. We have used 5 and 10 wt % carbon on the Li_2S particles (Supporting Information Figure S2), and the 10 wt % C coating provided better cycling stability than the 5 wt % coating. So all the Li_2S spheres were coated with 10 wt % carbon by CVD coating at 450 °C for 1.5 h.

Compared with the Li_2S-500 °C material, no obvious change was found in the XRD patterns for the Li_2S@C powder. However, the intensity of the Li_2S peak in the Raman spectrum decreased. As shown in Figure 1c, the Li_2S peak in the Li_2S@C material is reduced in intensity, which demonstrates that the carbon shell covered most of the Li_2S-core and blocked the Raman signal of Li_2S. The steps in the procedure for preparing the Li_2S@C core−shell particles are summarized in Figure 1d.

Figure 2 shows the SEM images of the three sizes of Li_2S spheres, with typical sizes of ~2 μm, 1 μm, and 500 nm, and their corresponding Li_2S@C core−shell particles. When

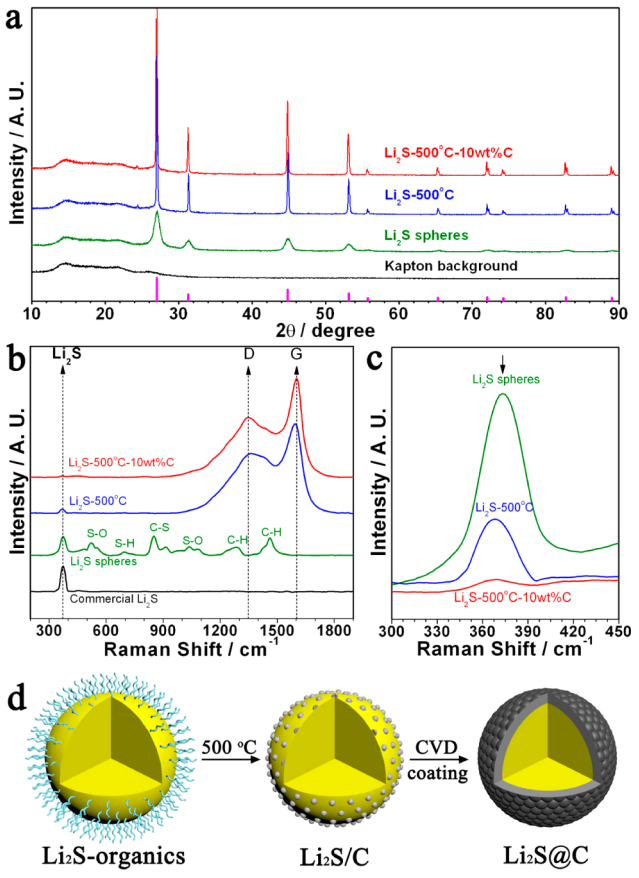

Figure 1. XRD and Raman characterization of as-synthesized Li_2S spheres. (a) XRD patterns and (b) Raman spectrum of Li_2S spheres, Li_2S spheres treated at 500 °C and Li_2S@C by further coated Li_2S-500 °C sample with 10 wt % carbon from CVD method; (c) Magnification of the Raman spectrum between 300 cm^{-1} and 450 cm^{-1}. (d) Schematic of the coating process for the Li_2S@C spheres.

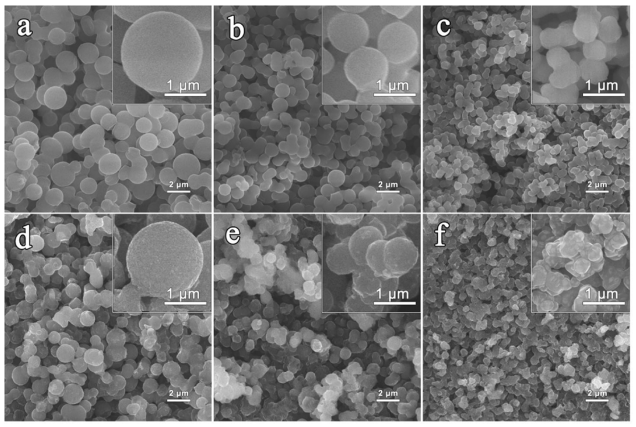

Figure 2. SEM images of the Li_2S spheres before and after CVD coating. (a) 2 μm Li_2S; (b) 1 μm Li_2S; (c) 500 nm Li_2S; (d) 2 μm Li_2S@C; (e) 1 μm Li_2S@C; (f) 500 nm Li_2S@C.

dx.doi.org/10.1021/ja412943h | J. Am. Chem. Soc. 2014, 136, 4659−4663

synthesizing these Li_2S spheres, both the heat treatment and the use of toluene played very important roles (see Supporting Information Figure S3). The particles assume a spherical shape due to the combination of small droplet size of the liquid dispersion, the elevated temperature, and the limited solubility of Li_2S. We have observed that, without the elevated temperature, spherical particles are not formed (Supporting Information Figure S3b). Toluene dissolves S and thus a liquid droplet dispersion is formed. According to our observations, THF has a higher solubility for Li_2S than does toluene, so when the heat treatment is applied, the THF slowly evaporates and stable Li_2S spheres are formed in toluene (Supporting Information Figure S4). The sizes of the Li_2S spheres were related to the amount of toluene used in the preparation; the particle sizes are as shown in Figure 2a–c. With the same amount of dissolved S (2 mmol), the largest amount of toluene (6 mL) gives the largest spherical Li_2S size of 2 μm, while the 3.5 and 3 mL toluene amounts form 1 μm and 500 nm Li_2S spheres respectively. When the obtained Li_2S spheres are further converted to Li_2S@C particles by CVD coating, volume shrinkage and roughening of the surface can be observed for these Li_2S spheres, as shown in Figure 2d–f. For the 2 and 1 μm Li_2S spheres, their morphologies do not change much after carbon coating. But for the 500 nm Li_2S spheres, many Li_2S particles are obviously linked together, showing some agglomeration after heat treatment.

To confirm the core–shell structure of the Li_2S@C spheres, an electron energy loss spectroscopy (EELS) line scan across a typical Li_2S@C sphere was performed, and the normalized EELS intensities of its S–L and C–K peaks were analyzed, as shown in Figure 3. The results show the Li_2S@C sphere to be a

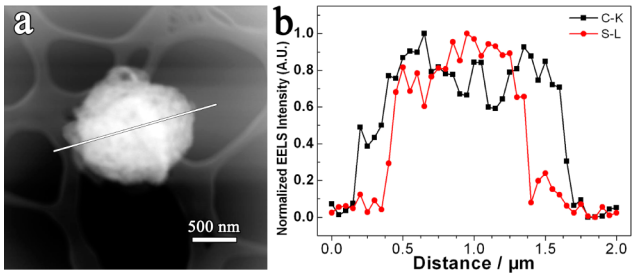

Figure 3. EELS characterization of the Li_2S@C sphere. (a) STEM image of a Li_2S@C sphere and (b) normalized EELS intensity along the line in (a).

typical core–shell structure, in which carbon covers the surface of the Li_2S sphere. The stable core–shell structure was also demonstrated by a polysulfide dissolution test on a large number of Li_2S@C spheres (Supporting Information Figure S5). These observations indicate the successful synthesis of carbon-coated Li_2S core–shell spheres by the CVD coating of carbon on Li_2S spheres. The thickness of the carbon coating for the 1 μm core–shell Li_2S@C spheres was analyzed by TEM and found to be about 30 nm (Supporting Information Figure S6).

The electrochemical performance of these three Li_2S@C (10 wt % C) materials were evaluated in coin cells, all under the same conditions. Figure 4a shows the discharge capacities of the 2 μm, 1 μm, and 500 nm Li_2S@C spheres at the 0.5C rate (1C = 1166 mA g^{-1} Li_2S). All of the electrodes were first charged to 4.0 V at the 0.05C rate to activate the cathodes[34] and then cycled between 1.5 and 2.8 V at the 0.5C rate. All cells show a

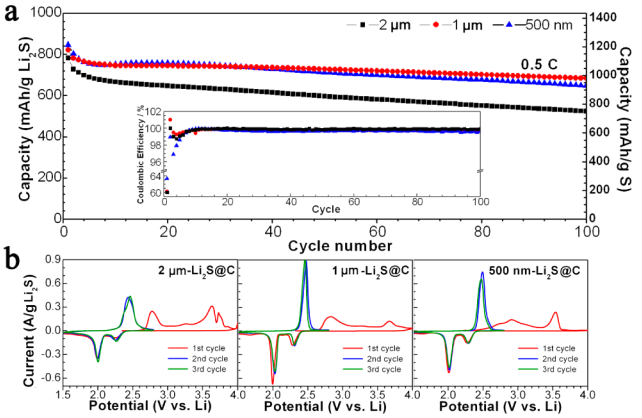

Figure 4. Cycling performance and cyclic voltammograms of the Li_2S@C materials of different sizes. (a) Cycling performances of the 2 μm, 1 μm, and 500 nm Li_2S@C particles at the 0.5C rate. (b) Cyclic voltammograms of the as-prepared Li_2S@C cathodes at a scan rate of 0.025 mV/s (Electrode composition: Li_2S@C/C/PVP = 66.7:28.3:5 by weight; 60 wt % Li_2S, 1.0–1.5 mg Li_2S/cm^2).

high Coulombic efficiency resulting from the small and uniform particle sizes as well as the protection provided by the stable carbon shell of these Li_2S@C spheres. The material structure has a strong influence on the performance, with both particle size and structure (C-coating) having a strong influence on both utilization and cycling stability. The cycling performances of uncoated Li_2S spheres, commercial Li_2S, and carbon-coated milled-commercial Li_2S under the same conditions are shown in the Supporting Information Figure S7. Compared with the uncoated Li_2S spheres, the cycling stability of the 1 μm Li_2S@C spheres is better, which reflects the effect of the carbon-shell protection. Compared with the carbon-coated milled-commercial Li_2S, the 1 μm Li_2S@C spheres show both better cycling stability and higher utilization. This may be the case because the spherical shape and small size provide the shortest diffusion distances compared with the other particles. Also, the spherical structure is geometrically strong which is beneficial for the stability of the Li_2S@C spheres during cycling. Among these three synthesized Li_2S@C materials, the electrochemical utilization of the 2 μm Li_2S is the lowest, which gives the lowest specific capacity. The 500 nm Li_2S@C and 1 μm Li_2S@C electrodes show very similar performance during the first 30 cycles, but the 500 nm Li_2S@C spheres with the smallest sizes show a faster capacity fading rate than that of the 1 μm Li_2S@C. The lower performance for the 500 nm particles presumably was caused by the longer Li diffusion distances introduced by the agglomeration as observed in Figure 2f. Similar results have also been observed for the rate capabilities of the three sizes of Li_2S@C particles (Supporting Information Figure S8). With both size and agglomeration effects taken into consideration, the 1 μm sample provides the best performance.

In order to analyze the effect of agglomeration of Li_2S particles, the cyclic voltammetry (CV) curves of the three Li_2S@C cathodes were compared as shown in Figure 4b. As for the commercial Li_2S, the pristine particles with large particle sizes (Supporting Information Figure S9) usually exhibit initial charge peaks at high voltages[34] and after being ball-milled the initial charge peaks shift to a lower voltage because of the reduced particle size[39] (Supporting Information Figure S10). By comparing the initial charge peaks of the three sizes of synthesized Li_2S@C particles, it is possible to see the effect of

dx.doi.org/10.1021/ja412943h | J. Am. Chem. Soc. 2014, 136, 4659–4663

the size changes resulting from agglomeration. For the as-synthesized 2 μm Li_2S@C material, there are three peaks in the first charge curve. In addition to the one charge peak below 3.5 V, there are two other peaks above 3.5 V. Regarding the 1 μm Li_2S@C and 500 nm Li_2S@C materials, although both of them show two peaks in the first charge curves, the 500 nm Li_2S@C actually showed more capacity above 3.5 V. Since more energy is needed for the larger particles to overcome the barrier of lithium extraction, it is reasonable to conclude that the charge capacity at the higher voltage reflects longer Li diffusion distances. Therefore, for the 500 nm Li_2S@C material, although the primary 500 nm Li_2S spheres have the smallest particle size, this advantage was compromised because of significant agglomeration as a result of the high temperature treatment. It should also be noted that the cathodic and anodic peaks below 2.6 V are the sharpest for the 1 μm material, indicative of the highest rate of Li uptake and release. Finally, the 1 μm Li_2S@C particles with less agglomeration have the best performance among the three synthesized Li_2S@C materials. Considering all the electrochemical performance data of the three Li_2S@C composites, it can be concluded that Li_2S@C with a small particle size and less agglomeration is the best configuration for Li/S cells.

The 1 μm Li_2S@C cathodes were cycled at different C-rates as shown in Figure 5a. The cells showed good capacity

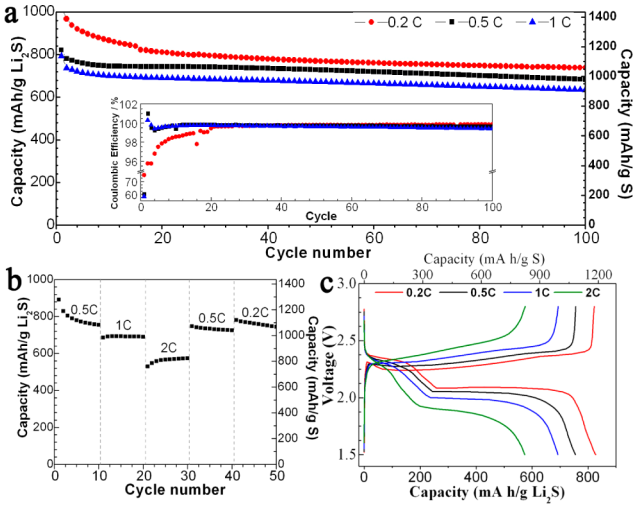

Figure 5. Electrochemical performance of the 1 μm Li_2S@C spheres at different C-rates. (a) Cycling performances and Coulombic efficiency of the 1 μm Li_2S@C cathodes at 0.2C, 0.5C, and 1C rates. (b) Rate capability of the 1 μm Li_2S@C cathodes. (c) Voltage profiles of the 1 μm Li_2S@C spheres at different C-rates (Electrode composition: Li_2S@C/C/PVP = 66.7:28.3:5 by weight; 60 wt % Li_2S, 1.0−1.5 mg Li_2S/cm^2).

retention. The initial specific capacity for the 1 μm Li_2S@C spheres cathode at the 0.2C rate is 972 mAh g^{-1} Li_2S (1394 mAh g^{-1} S), 821 mAh $g^{-1}Li_2S$ (1177 mAh g^{-1}S) at the 0.5C rate, and 793 mAh $g^{-1}Li_2S$ (1137 mAh g^{-1}S) at the 1C rate. After 100 cycles, the 1 μm particles can achieve a high specific capacity of 737 mAh g^{-1} Li_2S (1056 mAh g^{-1} S) at the 0.2C rate, 683 mAh g^{-1} Li_2S (979 mAh g^{-1} S) at the 0.5C rate, and 634 mAh g^{-1} Li_2S (909 mAh g^{-1} S) at the 1C rate with a Li_2S content of 60 wt % in the electrodes.

The rate capability of the 1 μm Li_2S@C cathodes is shown in Figure 5b. A highly reversible capacity of 570 mAh g^{-1} Li_2S could still be achieved even at the 2C rate, and when the C-rate was switched back to 0.5C again, the capacity recovered, indicating fast reaction kinetics in the cathodes. Representative voltage profiles of the 1 μm Li_2S@C cycled at different rates are shown in Figure 5c. All curves show highly reversible capacities.

The performance of an electrode with 1 μm Li_2S@C material and a high Li_2S weight percentage (electrodes with no added carbon black) was evaluated as shown in Figure 6. The rod-like

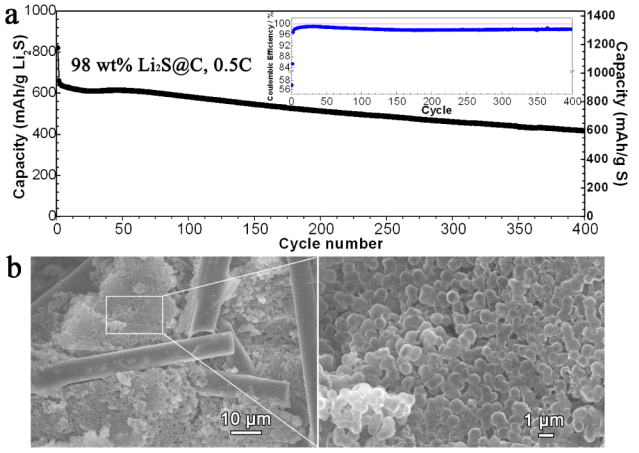

Figure 6. (a) Cycling performance of the 1 μm Li_2S@C electrode with no added carbon and 98 wt % Li_2S@C spheres at 0.5C. (b) SEM images of the electrode after 400 cycles (Electrode composition: Li_2S@C/SBR = 98:2 by weight; 88 wt % Li_2S, 1.1 mg Li_2S/cm^2).

structures in Figure 6b are the carbon fibers comprising the carbon fiber paper (Supporting Information Figure S11). As the electrode mixture is deposited in the pores of the paper, the carbon fiber paper acts as a 3D conductive network which links all the particles together and may increase the overall conductivity of the electrode. Thus even with no added carbon black, the 98 wt % Li_2S@C cells exhibited stable cycling performance with a high discharge capacity of 659 mAh g^{-1} Li_2S (945 mAh g^{-1} S) in the second cycle and a capacity of 417 mAh g^{-1} Li_2S (600 mAh g^{-1} S) after 400 cycles at 0.5C, as shown in Figure 6a. The modest capacity fading for this material may result from isolation of some active materials inside the core−shell structure. During the cycling of the Li_2S@C cell, the Li_2S particles are converted to sulfur when the cell is fully charged, corresponding to a volume shrinkage of ∼57% inside the carbon shell. So some sulfur might lose contact with the carbon shell after long-term cycling which causes the capacity fading for the Li_2S@C electrodes. After the cycling test, the electrode was removed from the cell, and the morphology of the Li_2S@C core−shell particles was examined by SEM as shown in Figure 6b. A few broken spheres can be found in the electrode, but most of the Li_2S@C particles show little morphology change after 400 cycles which is consistent with the good cyclability of the cell. These results show that the 1 μm Li_2S@C core−shell particles are stable in the cell and are suitable materials for Li/S cells.

■ CONCLUSION

In summary, for the first time, we report an easy synthesis strategy for the preparation of Li_2S spheres with size control and a CVD method for converting these Li_2S spheres to Li_2S@C core−shell particles. As Li_2S is in its maximum volume state in the Li/S cells, the carbon shells of the Li_2S@C core−shell particles are quite stable which helps to protect Li_2S from

dx.doi.org/10.1021/ja412943h | J. Am. Chem. Soc. 2014, 136, 4659−4663

dissolution as polysulfides and thus alleviates capacity fading. Preliminary results show that the Li_2S@C core−shell particles deliver both high specific capacity and stable cycling performance. Even with no added carbon, excellent electrochemical performance and a long cycle life can be achieved using a very high Li_2S content (88 wt % Li_2S) electrode composed of 98 wt % 1 μm Li_2S@C spheres and 2 wt % binder. Little morphology change of the 1 μm Li_2S@C particles was observed after 400 cycles. These results indicate that the core−shell structure reported here is stable and, therefore, a suitable configuration for Li/S cells. Considering the simple synthesis strategy and the unique particle morphology, the pristine Li_2S spheres can be used in combination with a variety of coating methods and different kinds of coating materials.

■ ASSOCIATED CONTENT

Supporting Information

Experimental details for the preparation of Li_2S and Li_2S@C spheres with three different sizes; electrochemical and materials characterization; XRD pattern of Li_2S@C at 700 °C; cycle performance of Li_2S@C with 5 wt % C; SEM images of products with different synthesis conditions; SEM images of particles obtained with different amounts of toluene at different times; morphology of the Li_2S@C materials after polysulfide dissolution tests; TEM analysis of Li_2S@C spheres before and after dissolving Li_2S; cycling performance of uncoated Li_2S spheres, commercial Li_2S, and carbon-coated milled-commercial Li_2S; rate performances of all three sizes of Li_2S@C particles; SEM image of commercial Li_2S; CVs of commercial Li_2S before and after milling; SEM images of carbon fiber paper before and after drop casting. This material is available free of charge via the Internet at http://pubs.acs.org.

■ AUTHOR INFORMATION

Corresponding Author

ejcairns@lbl.gov

Notes

The authors declare no competing financial interest.

■ ACKNOWLEDGMENTS

We thank Tevye Kuykendall and the LBNL Molecular Foundry for supporting the CVD coating work and Vincent Battaglia for the use of laboratory facilities. Thanks also go to Jaroslaw Syzdek and Robert Kostecki for help with the Raman characterization. Helpful discussions with Bruno Scrosati are appreciated. Caiyun Nan acknowledges a fellowship from the China Scholarship Council to perform this work at UC Berkeley and LBNL.

■ REFERENCES

(1) Armand, M.; Tarascon, J. M. *Nature* **2008**, *451*, 652.
(2) Goodenough, J. B.; Kim, Y. *Chem. Mater.* **2009**, *22*, 587.
(3) Choi, N.-S.; Chen, Z.; Freunberger, S. A.; Ji, X.; Sun, Y.-K.; Amine, K.; Yushin, G.; Nazar, L. F.; Cho, J.; Bruce, P. G. *Angew. Chem., Int. Ed.* **2012**, *51*, 9994.
(4) Bruce, P. G.; Freunberger, S. A.; Hardwick, L. J.; Tarascon, J.-M. *Nat. Mater.* **2012**, *11*, 19.
(5) Evers, S.; Nazar, L. F. *Acc. Chem. Res.* **2012**, *46*, 1135.
(6) Manthiram, A.; Fu, Y.; Su, Y.-S. *Acc. Chem. Res.* **2012**, *46*, 1125.
(7) Zhang, C.; Wu, H. B.; Yuan, C.; Guo, Z.; Lou, X. W. *Angew. Chem.* **2012**, *124*, 9730.
(8) Wang, H.; Yang, Y.; Liang, Y.; Robinson, J. T.; Li, Y.; Jackson, A.; Cui, Y.; Dai, H. *Nano Lett.* **2011**, *11*, 2644.
(9) Ji, L.; Rao, M.; Zheng, H.; Zhang, L.; Li, Y.; Duan, W.; Guo, J.; Cairns, E. J.; Zhang, Y. *J. Am. Chem. Soc.* **2011**, *133*, 18522.
(10) Xin, S.; Gu, L.; Zhao, N.-H.; Yin, Y.-X.; Zhou, L.-J.; Guo, Y.-G.; Wan, L.-J. *J. Am. Chem. Soc.* **2012**, *134*, 18510.
(11) Li, W.; Zheng, G.; Yang, Y.; Seh, Z. W.; Liu, N.; Cui, Y. *Proc. Natl. Acad. Sci. U.S.A.* **2013**, *110*, 7148.
(12) Zhou, W.; Yu, Y.; Chen, H.; DiSalvo, F. J.; Abruña, H. D. *J. Am. Chem. Soc.* **2013**, *135*, 16736.
(13) Wei Seh, Z.; Li, W.; Cha, J. J.; Zheng, G.; Yang, Y.; McDowell, M. T.; Hsu, P.-C.; Cui, Y. *Nat. Commun.* **2013**, *4*, 1331.
(14) Wu, F.; Chen, J.; Chen, R.; Wu, S.; Li, L.; Chen, S.; Zhao, T. *J. Phys. Chem. C* **2011**, *115*, 6057.
(15) Jayaprakash, N.; Shen, J.; Moganty, S. S.; Corona, A.; Archer, L. A. *Angew. Chem.* **2011**, *123*, 6026.
(16) Ji, X.; Nazar, L. F. *J. Mater. Chem.* **2010**, *20*, 9821.
(17) Ji, X.; Lee, K. T.; Nazar, L. F. *Nat. Mater.* **2009**, *8*, 500.
(18) Song, M.-K.; Zhang, Y.; Cairns, E. *J. Nano Lett.* **2013**, *13*, 5891.
(19) Zheng, G.; Yang, Y.; Cha, J. J.; Hong, S. S.; Cui, Y. *Nano Lett.* **2011**, *11*, 4462.
(20) Zheng, S.; Chen, Y.; Xu, Y.; Yi, F.; Zhu, Y.; Liu, Y.; Yang, J.; Wang, C. *ACS Nano* **2013**, *7*, 10995.
(21) Elazari, R.; Salitra, G.; Garsuch, A.; Panchenko, A.; Aurbach, D. *Adv. Mater.* **2011**, *23*, 5641.
(22) Guo, J.; Xu, Y.; Wang, C. *Nano Lett.* **2011**, *11*, 4288.
(23) Lee, J. T.; Zhao, Y.; Thieme, S.; Kim, H.; Oschatz, M.; Borchardt, L.; Magasinski, A.; Cho, W.-I.; Kaskel, S.; Yushin, G. *Adv. Mater.* **2013**, *25*, 4573.
(24) Zhang, K.; Zhao, Q.; Tao, Z.; Chen, J. *Nano Research* **2013**, *6*, 38.
(25) Moon, S.; Jung, Y. H.; Jung, W. K.; Jung, D. S.; Choi, J. W.; Kim, D. K. *Adv. Mater.* **2013**, *25*, 6547.
(26) Li, W.; Zhang, Q.; Zheng, G.; Seh, Z. W.; Yao, H.; Cui, Y. *Nano Lett.* **2013**, *13*, 5534.
(27) Su, Y.-S.; Manthiram, A. *Nat. Commun.* **2012**, *3*, 1166.
(28) Chung, S.-H.; Manthiram, A. *Adv. Mater.* **2013**, DOI: 10.1002/adma.201304365.
(29) Liang, X.; Wen, Z.; Liu, Y.; Wu, M.; Jin, J.; Zhang, H.; Wu, X. *J. Power Sources* **2011**, *196*, 9839.
(30) Suo, L.; Hu, Y.-S.; Li, H.; Armand, M.; Chen, L. *Nat. Commun.* **2013**, *4*, 1481.
(31) Marmorstein, D.; Yu, T. H.; Striebel, K. A.; McLarnon, F. R.; Hou, J.; Cairns, E. J. *J. Power Sources* **2000**, *89*, 219.
(32) Zhang, S. S.; Tran, D. T. *Electrochim. Acta* **2013**, *114*, 296.
(33) Seh, Z. W.; Zhang, Q.; Li, W.; Zheng, G.; Yao, H.; Cui, Y. *Chem. Sci.* **2013**, *4*, 3673.
(34) Fu, Y.; Su, Y.-S.; Manthiram, A. *Adv. Energy Mater.* **2013**, DOI: 10.1002/aenm.201300655.
(35) Yang, Y.; Zheng, G.; Misra, S.; Nelson, J.; Toney, M. F.; Cui, Y. *J. Am. Chem. Soc.* **2012**, *134*, 15387.
(36) Yang, Y.; McDowell, M. T.; Jackson, A.; Cha, J. J.; Hong, S. S.; Cui, Y. *Nano Lett.* **2010**, *10*, 1486.
(37) Hassoun, J.; Sun, Y.-K.; Scrosati, B. *J. Power Sources* **2011**, *196*, 343.
(38) Hassoun, J.; Scrosati, B. *Angew. Chem., Int. Ed.* **2010**, *49*, 2371.
(39) Cai, K.; Song, M.-K.; Cairns, E. J.; Zhang, Y. *Nano Lett.* **2012**, *12*, 6474.
(40) Guo, J.; Yang, Z.; Yu, Y.; Abruña, H. D.; Archer, L. A. *J. Am. Chem. Soc.* **2012**, *135*, 763.
(41) Jeong, S.; Bresser, D.; Buchholz, D.; Winter, M.; Passerini, S. *J. Power Sources* **2013**, *235*, 220.
(42) Hayashi, A.; Ohtsubo, R.; Tatsumisago, M. *Solid State Ionics* **2008**, *179*, 1702.
(43) Gladysz, J.; Wong, V. K.; Jick, B. S. *Tetrahedron* **1979**, *35*, 2329.
(44) Zhang, L.; Ji, L.; Glans, P.-A.; Zhang, Y.; Zhu, J.; Guo, J. *Phys. Chem. Chem. Phys.* **2012**, *14*, 13670.
(45) Barletta, R. E.; Gros, B. N.; Herring, M. P. *J. Raman Spectrosc.* **2009**, *40*, 972.